Inorganic Chemistry

Article

pubs.acs.org/IC

Metal- and Ligand-Assisted CO_2 Insertion into Ru−C, Ru−N, and Ru−O Bonds of Ruthenium(II) Phosphine Complexes: A Density Functional Theory Study

Prabha Vadivelu* and Cherumuttathu H. Suresh

Inorganic and Theoretical Chemistry Section, CST Division, CSIR-National Institute for Interdisciplinary Science and Technology, Trivandrum 695019, Kerala, India

Supporting Information

ABSTRACT: The CO_2 insertion reactions of [$L_4Ru(\eta^2$-$CH_2C_6H_4)$] (**1**), [$L_4Ru(\eta^2$-$OC_6H_3Me)$] (**2**), and [$L_4Ru(\eta^2$-$NHC_6H_4)$] (**3**), where L = PH_3 and PMe_3, are modeled using density functional theory methods. In **1** and **2**, the metal-assisted CO_2 insertion occurs because of the favorable initial axial phosphine dissociation mechanism, whereas in **3**, the ligand (NHC_6H_4)-assisted mechanism operates ($\Delta G^{\ddagger}$ = +19.0 kcal/mol), wherein the nucleophilic affinity of the $-NHC_6H_4$ moiety aids the CO_2 insertion process. The modeled mechanisms are consistent with the experimental findings by Hartwig et al. (*J. Am. Chem. Soc,* **1991**, 113, 6499), in which the rate of the reactions of **1** and **2** depends on the added phosphine concentration, whereas the rate of the reaction of **3** is independent of the added phosphine concentration. In **1** and **2**, CO_2 is preferably inserted into the Ru−C_{aryl} bond rather than the competitive Ru−CH_2 and Ru−O bonds, respectively. In **1**, the π-type orbital interaction of the aryl ring with the metal center is found to stabilize the transition state for Ru−C_{aryl} bond insertion ($\Delta G^{\ddagger}$ = +25.7 kcal/mol). In **2**, the Ru−C_{aryl} insertion ($\Delta G^{\ddagger}$ = +23.0 kcal/mol) is thermodynamically preferred, while the kinetically preferred Ru−O bond insertion ($\Delta G^{\ddagger}$ = +17.4 kcal/mol) is highly reversible. The more electron-donating and sterically bulky PMe_3 facilitates the CO_2 insertion of **1** and **2** because the initial dissociation of axial PMe_3 is easier than that of PH_3 by ca. +11.0 kcal/mol, whereas in the case of **3**, the effect of PMe_3 slightly increases the $\Delta G^{\ddagger}$ value of **3**. The increase in the nucleophilic affinity of amido nitrogen in **3** and the increase in the polarity of the solvent decrease the $\Delta G^{\ddagger}$ value of **3** by 48%. The inclusion of the chelating dimethylphosphinoethane ligand in **3** along with the electron-donating substituent at the $-NHC_6H_4$ moiety and the polar solvent further reduces the $\Delta G^{\ddagger}$ value of **3** by 62%, which demonstrates the role of the chelating ligand, electron-donating substituent, and polar solvent in the ligand-assisted CO_2 insertion reactions.

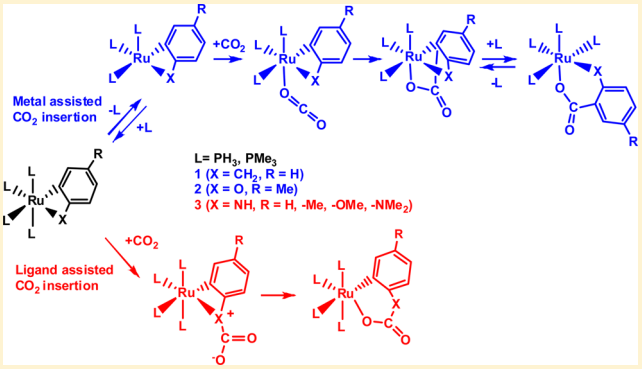

INTRODUCTION

In recent years, there is significant interest in the use of carbon dioxide (CO_2) as a chemical feedstock because of growing attention on environmental, legal, and social issues.[1] The activation and functionalization of CO_2 via a transition-metal center is well established and is of interest because of the possibility of utilizing CO_2 as an inexpensive 1-carbon fragment in synthesis.[2,3] An important step in the functionalization of CO_2 is its insertion into the metal (M)−E (E = C, H, N, O, P, Si) bonds, which produces a range of different products including carboxylates, formates, carbamates, carbonates, etc.[4−7] CO_2 insertion into an M−X bond (X = alkyl, alkoxide, amide, etc.) has been widely investigated with titanium,[8] zirconium,[8] niobium,[8] chromium,[9] tungsten,[9] rhenium,[10] palladium,[11] and copper.[12] However, examples of CO_2 insertion into the group 8 M−C, M−O, and M−N bonds are relatively rare.[7,13−16]

Previously, coordinatively unsaturated acetylide complex [Cp*Ru(PPh_3)(C≡CPh)] has been reported to react with CO_2 to produce the carboxylate complex [Cp*Ru(PPh_3)(η^2-$O_2CC{\equiv}CPh$)], in which CO_2 is inserted into the Ru−C bond.[17] Field et al. have also investigated the CO_2 insertion reactions into the Ru−C bonds of *cis*-[$Ru(DMPE)_2Me_2$] and *trans*-[$Ru(DMPE)_2Me_2$] complexes.[18] They found that the stereochemistry of the starting material is a key factor in determining the rate of the CO_2 insertion reaction, wherein the trans isomer reacted much more readily with CO_2 than the cis isomer and formed *trans*-[$Ru(DMPE)_2(OCOMe)Me$] and *trans*-[$Ru(DMPE)_2(OCOMe)_2$], respectively. The cis isomer produced*cis*-[$Ru(DMPE)_2(OCOMe)Me$] and *cis*-[$Ru(DMPE)_2(OCOMe)_2$], respectively. These results also indicate that the stereochemical integrity at the metal center is retained as insertion occurs.

The CO_2 insertion reaction into the Ru−O bond is very rare. Mandal and co-workers[19] found that the manganese(I) and

Received: September 16, 2014
Published: December 23, 2014

DOI: 10.1021/ic5022577
Inorg. Chem. 2015, 54, 502−512

rhenum(I) alkoxide complexes of *fac*-[$M(CO)_3(P{-}P)(OR)$] (M = Mn or Re; P−P = dppe or dppp; R = CH_3 or CF_3CH_2) undergo CO_2 insertion into the M−O bond at room temperature to form the carbonate complexes *fac*-[$M(CO)_3(P{-}P)(O_2COR)$].[19] It is also found that benzene solutions of these alkoxide complexes are capable of absorbing CO_2 from the atmosphere. The insertion and deinsertion of CO_2 from these complexes are reversible under mild conditions.

The CO_2 insertion reactions with metal−amido species to form metal carbamato complexes are known,[20] particularly for the early transition metals. Only a few reports are available for such reactions in the case of late transition metals. A rare example involving the *trans*-[$Pt(PCy_3)_2(Ph)(NH_2)$] complex was found to undergo CO_2 insertion into the Pt−N bond.[21] Early in 2012, Maseras et al.[22] have investigated the CO_2 insertion reactions of nickel amido species supported by a PCP ligand and found that CO_2 insertion occurs in the Ni−N bond to form the N-bound carbamato species, which would rearrange to form the final O-bound product. The same group also carried out the CO_2 insertion reaction of cyclometalated [(κ^2-*N*,*N*-2-NHC_5NH_4)$IrH_2(PPh_3)_2$] species and found that CO_2 insertion takes place in the Ir−N bond to form the carbamato [(κ^2-*O*,*N*-2-$OC(O)NHC_5NH_4$)$IrH_2(PPh_3)_2$] species.[23] In this study, it was demonstrated that the rate of the reaction depends on the nucleophilicity of amide species; with more nucleophilic amides, much faster insertions were observed.

The theoretical studies on the mechanism of CO_2 insertion into an M−X bond (X = hydroxide, alkoxide, amide, etc.)[24−27] are very limited, and these limited studies demonstrated that the CO_2 molecule is activated by the lone pair(s) of electrons of X. In 1995, Sakaki and Musashi[25] modeled the CO_2 insertion into the Cu−OH bond of [$L_2Cu(OH)$] (L = PH_3) complex and found that CO_2 insertion occurs because of the strong bonding interaction of the lone-pair p orbital of OH with one of the CO_2 π^* orbitals. Recently, in 2012, Schmeier et al.[26] synthesized the [(PCP)Ni(X)] [X = NH_2 and OH; PCP = 2,6-$C_6H_3(CH_2PMe_2)_2$] complex and theoretically investigated the CO_2 insertion mechanism into the Ni−X bond. They showed that CO_2 insertion takes place by the nucleophilic attack of ligand X on the carbon atom of CO_2 followed by a rearrangement to the insertion product. The rearrangement was calculated to be the rate-determining step.

In fact, very few literatures studied the competitive reactivity of the M−H, M−C, M−O, and M−N bonds for CO_2 insertion reactions. In this context, Field et al.[18] reported the CO_2 insertion into the Ru−C or Ru−H bonds of *trans*-[$Ru(DMPE)_2MeH$] species. Although the insertion reaction was more facile for the Ru−H bond than Ru−C, a thermodynamically stable Ru−C-inserted product *trans*-[$Ru(DMPE)_2(O_2CMe)(H)$] was observed, suggesting a rapid deinsertion of CO_2 from *trans*-[$Ru(DMPE)_2(Me)(O_2CH)$], the Ru−H-inserted product. In a similar study using a cyclometalated [$RuH(\eta^2$-$CH_2PMe_2)(PMe_3)_3$] complex, Field et al. reported the relative reactivity of the Ru−H and Ru−C bonds with respect to CO_2 insertion.[28] They found that CO_2 inserts into the Ru−C bond with the apparent absence of any observable CO_2 insertion into the Ru−H bond. It again suggests that metal hydride insertions and subsequent decarboxylation are too fast to observe on the NMR time scale.[28]

A comparative study for the insertion of CO_2 into the Ru−C, Ru−O, and Ru−N bonds has been carried out by Hartwig et al.[29] for three related complexes, [$L_4Ru(\eta^2$-$CH_2C_6H_4)$] (**1**), [$L_4Ru(\eta^2$-$OC_6H_3Me)$] (**2**), [$L_4Ru(\eta^2$-$NHC_6H_4)$] (**3**), where L = PMe_3. The reaction of **1** with 1 equiv of CO_2 at 85 °C in toluene led predominantly the Ru−C_{aryl}-inserted product (Scheme 1), whereas the Ru−C_{alkyl} insertion product was not

Scheme 1. CO_2 Insertion Reaction of 1−3, Where L = PMe_3

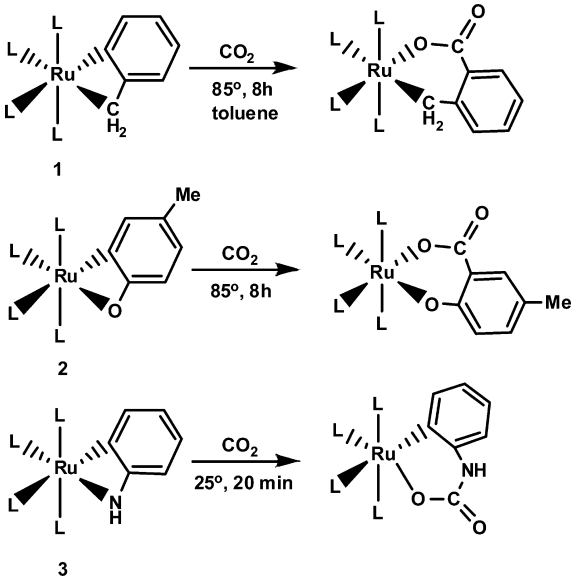

observed. The reaction is found to be very similar for **2** with 1 equiv of CO_2 at 85 °C because the resulting product was due to Ru−C_{aryl} bond insertion of CO_2. The Ru−O-bond-inserted product was conspicuous by its absence because one would expect that the mismatch of a soft late-transition-metal center and a hard phenoxide substituent would lead to the preferential Ru−O bond insertion rather than the Ru−C_{aryl} bond insertion.[30−32] However, similar to **2**, the preferential M−C bond over the M−O bond insertion was reported in the case of carbon monoxide insertion reactions.[33,34] The rate of Ru−C_{aryl} bond insertions in both **1** and **2** showed a marked dependence on the added phosphine concentration. In contrast to **1** and **2**, the reaction of **3** with CO_2 has led to the formation of a Ru−N-inserted product, wherein the Ru−C_{aryl} bond insertion does not exist. The preferred Ru−N bond insertion in **3** may be due to the weaker Ru−N bond than the Ru−C_{aryl} bond. Also, unlike **1** and **2**, complex **3** exhibits no dependency of the rate on the added phosphine concentration. All of these suggested a different mechanism for the CO_2 insertion of **3** compared to that of **1** and **2**.

For complexes **1** and **2**, the marked decrease in the rate observed for samples containing added phosphine prompted Hartwig et al. to suggest the mechanism in Scheme 2. This mechanism involves an initial reversible phosphine dissociation that creates a vacant site on the metal for CO_2 coordination. In the next steps, coordination of CO_2 followed by migration of the aryl group leads to the CO_2-inserted product. Finally, the reversible phosphine addition takes place to form the product. In contrast to **1** and **2**, the reaction of **3** with CO_2 was found to occur without prior phosphine dissociation (due to labeling studies on phosphines and no dependency of the rate on the phosphine concentration), and it was postulated that the reaction involved a direct nucleophilic attack of a nitrogen atom on CO_2 to form an N-bound carbamato species, which would rearrange to form the final O-bound product (Scheme 3).

DOI: 10.1021/ic5022577
Inorg. Chem. 2015, 54, 502−512

Scheme 2. Proposed Mechanism for CO_2 Insertion of 1 and 2, Where L = PMe_3

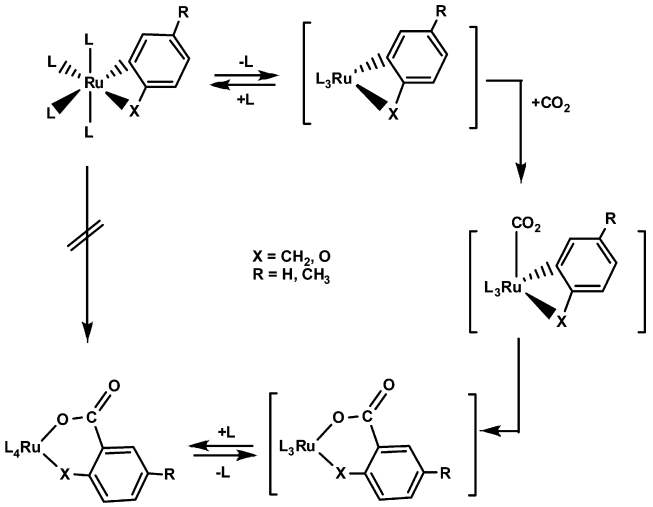

The experimental studies on the CO_2 insertion reactions of **1**–**3** clearly indicate the reactivity difference of the Ru–C_{aryl}, Ru–C_{alkyl}, Ru–O, and Ru–N bonds toward CO_2 insertion and also propose a different reaction mechanism for CO_2 insertion to **3** than **1** and **2**. However, the detailed mechanistic insights of these reactions and the explanation for the different reactivities of the Ru–C, Ru–O, and Ru–N bonds are not well identified. The intriguing aspects are as follows: (i) Why is CO_2 preferably inserted into the Ru–C_{aryl} bond of **1** rather than the weaker Ru–C_{alkyl} bond. (ii) Although **2** has a weaker Ru–O bond, why is CO_2 preferably inserted into the Ru–C_{aryl} bond. (iii) Similar to **1** and **2**, why is CO_2 not inserted into the Ru–C_{aryl} bond in **3**. Is this due to the proposed nucleophilic attack mechanism of a nitrogen atom of **3** on CO_2 rather than the initial phosphine dissociation mechanism? Herein we use density functional theory (DFT) methods to gain mechanistic insights of the CO_2 insertion reactions of **1**–**3** in terms of their modeled intermediates and energetics. We also made an attempt to modify complexes **1**–**3** using various ligands, substituents, and solvents to improve their efficacy toward CO_2 insertion reactions.

COMPUTATIONAL DETAILS

The structures of the complexes are fully optimized at the B3LYP level[35−37] of DFT using the *Gaussian09* program.[38] Ruthenium and phosphorus centers were described with the Stuttgart RECPs and associated basis sets (SDDALL)[39] with a set of d-orbital polarization functions on phosphorus (ζ = 0.387).[40] 6-31G** basis sets were used for all other atoms.[41,42] All stationary points were fully characterized via analytical frequency calculations as either minima (all positive eigenvalues) or transition states (one imaginary eigenvalue), and IRC calculations were used to confirm the minima linked by each transition state. Energies include a correction for zero-point energies, and free energies are quoted at 298.15 K. The single-point calculations of the B3LYP-optimized geometries were performed to incorporate the effect of various solvents such as toluene, tetrahydrofuran (THF), acetone, and acetonitrile via the polarized continuum model approach.[43−45] In order to validate the B3LYP method, nine other methods, viz., BLYP, BP86,[46,47] B3P86, PBEPBE,[48,49] PBE1PBE,[50] B3PW91,[51,52] M06,[53] M06L[54] and B97D,[55] have also been tested to find the activation barriers for complex **1**. In addition, the effect of the basis set on the activation barrier of **1** is tested via the single-point calculations of the B3LYP-optimized geometries by employing the SDDALL basis set for ruthenium and phosphorus and the 6-311++G** basis set for the rest of the atoms [B3LYP(6-311++G**)//B3LYP(6-31G**)]. The nine different methods and higher basis set calculations consistently reproduced the B3LYP results that CO_2 insertion into the Ru–C_{aryl} bond of **1** is kinetically more preferred than that into the Ru-CH_2 bond (Table S1 in the Supporting Information, SI). The coordination mode of the CO_2 molecule with the ruthenium center is also confirmed by two other methods, viz., B3LYP-D and M06, along with the B3LYP method. MESPs are calculated for selected complexes to quantify the nucleophilicity of the heteroatom.

RESULTS AND DISCUSSION

Small Model Systems. *i. CO_2 Insertion of 1.* The CO_2 insertion reaction of **1** has been modeled via a phosphine dissociative mechanism, as shown in Scheme 2. The optimized intermediates and transition states located for this mechanism are shown in Figure 1. The computed energy profile, which contains the relative free energy and relative electronic energy, is shown in Scheme 4. The relative free energies and relative electronic energies are similar in cases where the numbers of reactant and product molecules are equal, for example, two-to-two transformation, but differ significantly for two-to-three or two-to-one transformations because of the entropic contribution. The first step of the mechanism is phosphine ligand dissociation, which creates a vacant site for CO_2 coordination. Three possibilities exist for phosphine dissociation. The first possibility is dissociation of one of the symmetrically equivalent phosphines from the axial position. The other two possibilities can be described in terms of dissociation of the equatorial phosphines. The axial phosphine dissociation giving **4a** is energetically more favored than dissociation of the equatorial phosphines, by ca. +2.9 kcal/mol. In **1**, the mutually trans phosphines are found to be distorted from the axial coordination plane (the torsion angles of P1–Ru–P2–P4 and P1–Ru–P3–P4 are 170°) in order to minimize the steric hindrance of four phosphine ligands. Distortion of the axial phosphine can be attributed to the energetically preferred dissociation of the axial phosphine rather than the equatorial phosphines. In a comparison of the geometries of **1** and **4a**, the phenyl unit of the latter is more bent toward the metal center, giving rise to an additional Ru–C2 interaction (the Ru–C2

Scheme 3. Proposed Mechanism for CO_2 Insertion of 3, Where L = PMe_3

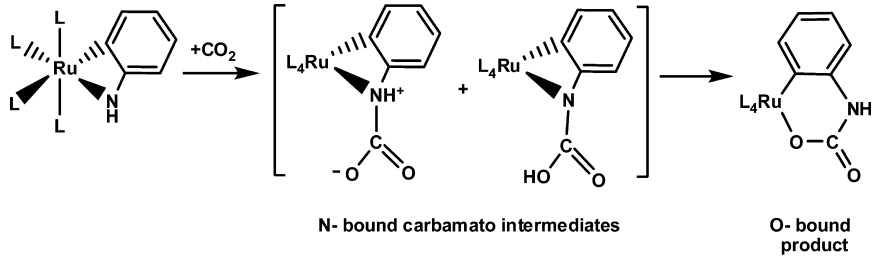

DOI: 10.1021/ic5022577
Inorg. Chem. 2015, 54, 502−512

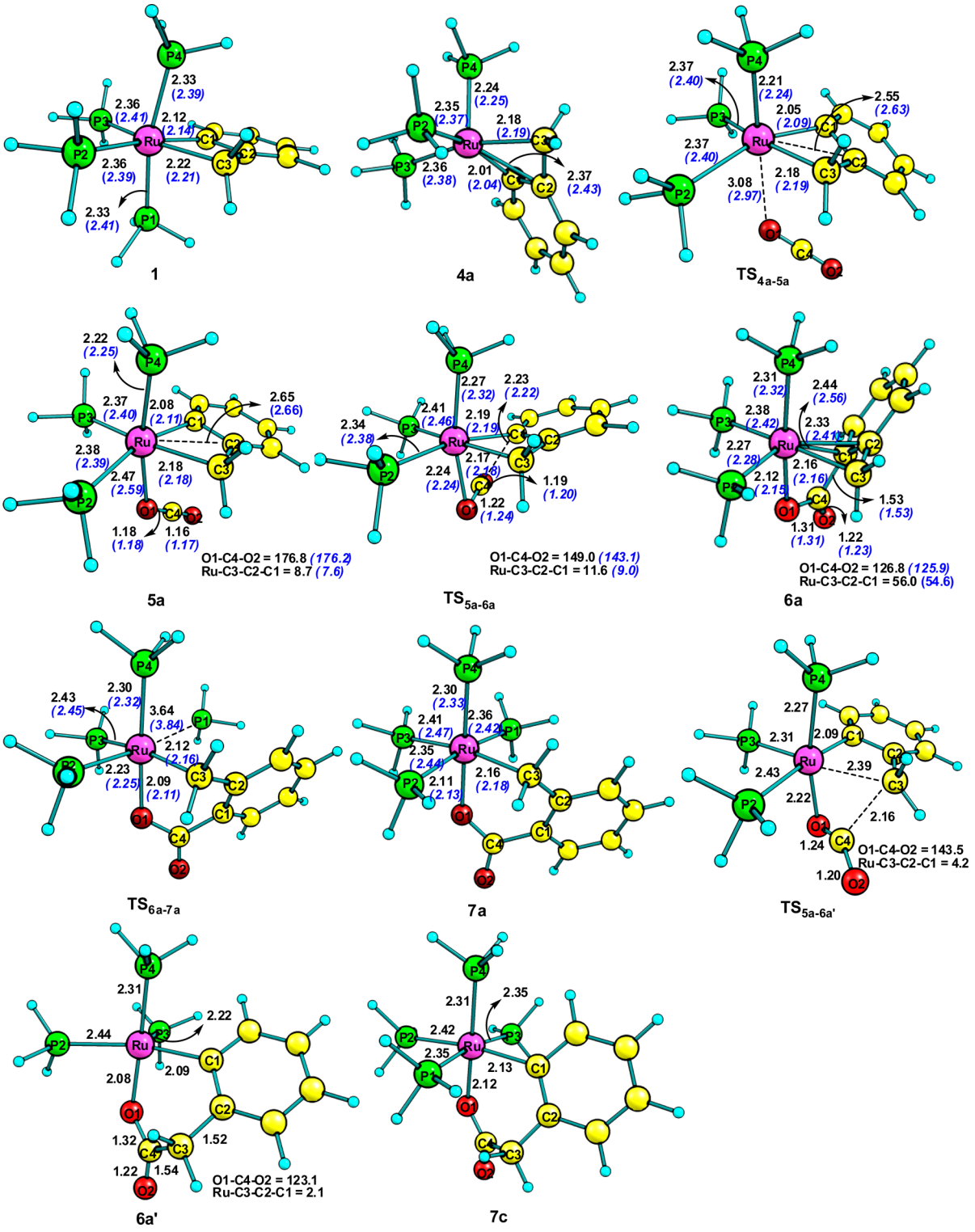

Figure 1. Optimized intermediates and transition states for CO_2 insertion into the Ru−C_{aryl} and Ru−CH_2 bonds of **1**, where L = PH_3/PMe_3. Selected distances are given in angstroms.

bond distance is 2.37 Å; cf. Figure 1). It is worth noting that a direct coordination of CO_2 to the vacant site of **4a** does not occur and instead it passes through the transition state TS_{4a-5a} with an activation free energy ($\Delta G^{\ddagger}$) of +16.6 kcal/mol to form **5a**. The moderately high $\Delta G^{\ddagger}$ again suggests that in **4a** the Ru−C2 interaction is significant and it has to be broken in order to accept the η^1 coordination of oxygen from CO_2 to the metal. The η^2 coordination of CO_2 with the ruthenium center and the η^1 coordination of CO_2 via the carbon atom are also tested in **5a** with two different methods, viz., B3LYP-D and M06, along with the B3LYP method, and all attempts to optimize such coordination geometries always led to **5a**.

From **5a**, CO_2 can be inserted either into the Ru−C_{aryl} bond or into the Ru−CH_2 bond. The CO_2 insertion into the Ru−C_{aryl} bond is associated with a transition state (TS_{5a-6a}; $\Delta G^{\ddagger}$ = +25.7 kcal/mol) which is +6.6 kcal/mol lower in energy than

DOI: 10.1021/ic5022577
Inorg. Chem. 2015, 54, 502−512

Scheme 4. Computed Free Energy Profile (kcal/mol) for CO_2 Insertion into the Ru−C_{aryl} and Ru−CH_2 Bonds of 1[a]

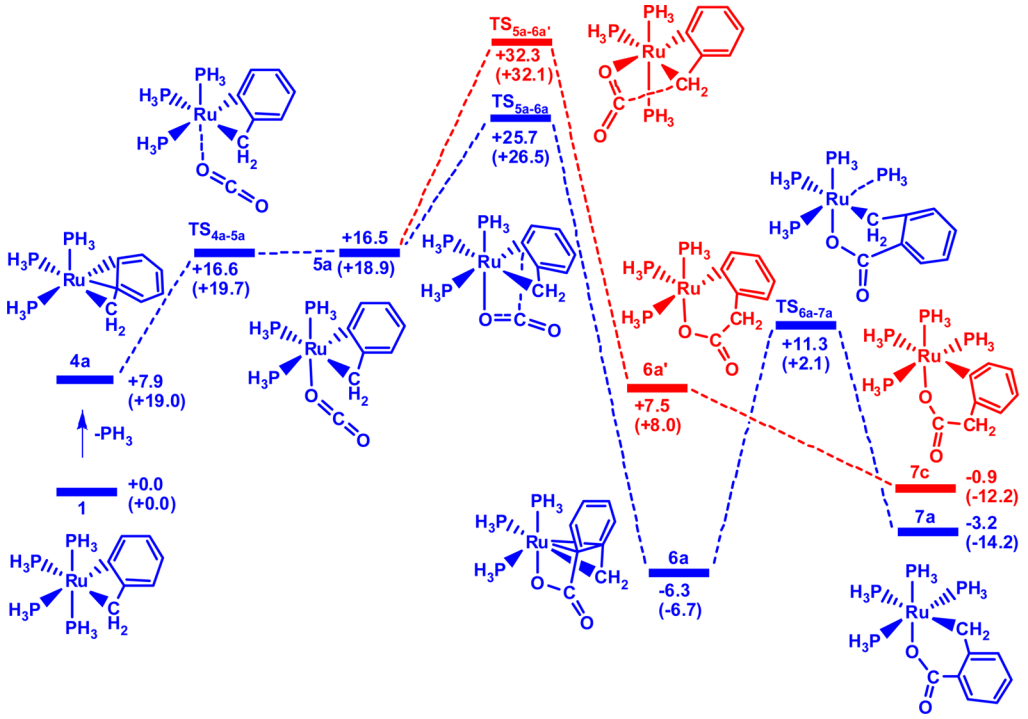

[a]Electronic energies (kcal/mol) are given in parentheses.

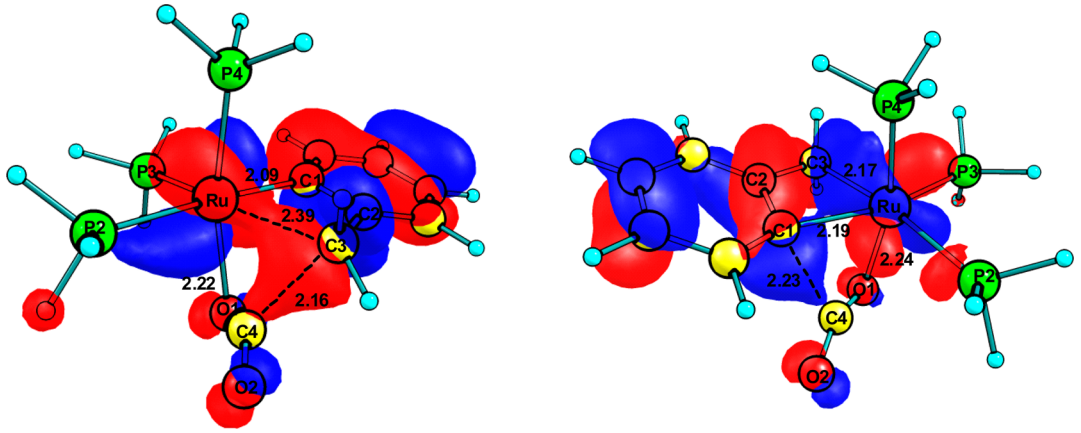

Figure 2. HOMO of transition states $TS_{5a-6a'}$ (left) and TS_{5a-6a} (right). The isosurface with the value of 0.035e is plotted.

the transition state ($TS_{5a-6a'}$) corresponding to the CO_2 insertion into the Ru−CH_2 bond. In $TS_{5a-6a'}$, the Ru−CH_2 σ bond (Ru−C3 = 2.39 Å) has to be almost completely broken to establish an interaction with the carbon of CO_2, whereas in TS_{5a-6a}, the Ru−C_{aryl} bond (2.19 Å) is almost intact because the interaction to the carbon of CO_2 is easily established from the π-type orbital of the phenyl ring (Figure 2). In other words, compared to $TS_{5a-6a'}$, TS_{5a-6a} shows an enhanced π-type orbital interaction of the phenyl ring with the metal center, and this results in an earlier transition state and lower $\Delta G^{\ddagger}$ for the CO_2 insertion into the Ru−C_{aryl} bond than that into the Ru−CH_2 bond. The CO_2 insertion into the Ru−C_{aryl} bond leads to an exothermic intermediate **6a**, while that into the Ru−CH_2 bond leads to an endothermic intermediate **6a′**. The higher stability of **6a** than **6a′** (by +13.8 kcal/mol) is due to the η^3 coordination of the aryl ring, and this coordination mode is not found in **6a′**. In the next step, the phosphine association to **6a** formed the thermodynamically more stable product **7a** (ΔG = −3.2 kcal/mol) via the transition state (TS_{6a-7a}; ΔG = +11.3 kcal/mol), whereas **6a′** leads directly to **7c** (ΔG = −0.9 kcal/mol). The computed energetics of **1** show that the CO_2 insertion into the Ru−C_{aryl} bond is kinetically and thermodynamically more preferred than that into the Ru−CH_2 bond. This is mostly because of the stabilizing π-type orbital interaction of the phenyl ring found for the Ru−C_{aryl} insertion than the Ru−CH_2 insertion, which stabilizes the intermediates and transition states associated with the Ru−C_{aryl} insertion.

There are instances in which the energetically preferred mechanism commences with the less stable intermediate species.[56−58] Thus, the CO_2 insertion mechanisms from less stable equatorial phosphine-dissociated intermediates **4b** and **4c** are also modeled, and details of the intermediates and energetics are shown in Figure S1 and Scheme S2 in the SI. The modeled pathways from these species are associated with the

DOI: 10.1021/ic5022577
Inorg. Chem. 2015, 54, 502−512

Scheme 5. Computed Free Energy Profile (kcal/mol) for CO_2 Insertion into the Ru−C_{aryl} and Ru−O Bonds of 2[a]

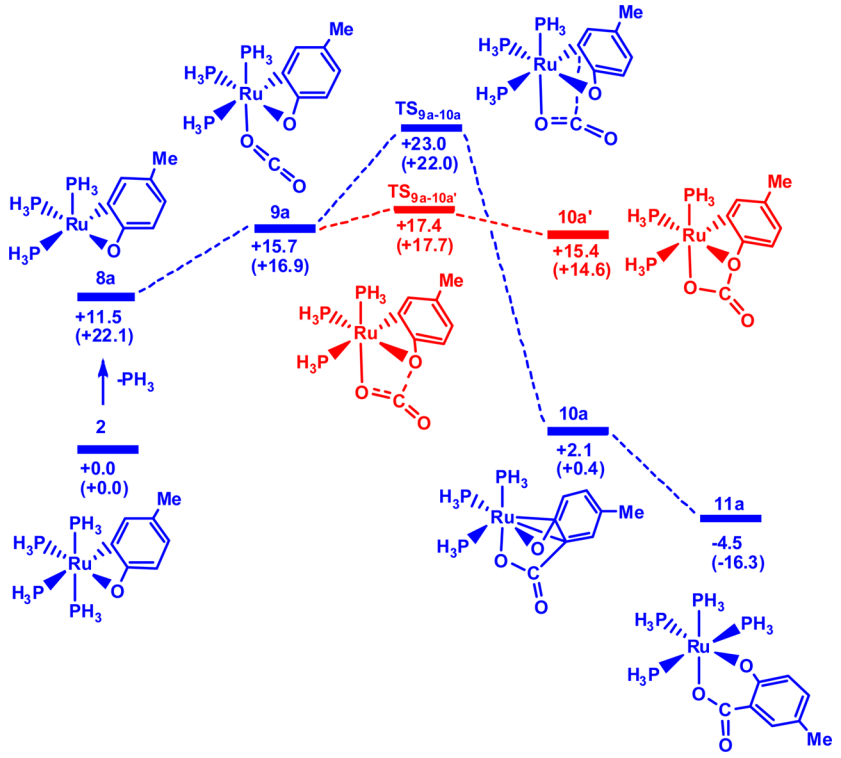

[a]Electronic energies (kcal/mol) are given in parentheses.

high-lying rate-determining transition states, higher by +13.0 to +18.0 kcal/mol than TS_{5a-6a}, and also they lead to thermodynamically more unstable CO_2 insertion products. Hence, it is clear that the initial axial phosphine dissociation from **1** proceeds via the more preferred CO_2 insertion mechanism to the Ru−C_{aryl} bond, while the equatorial phosphine dissociation does not lead to a favorable CO_2 insertion mechanism.

ii. CO_2 Insertion of 2. Similar to **1**, the axial phosphine dissociation of **2** giving **8a** (Scheme 5) is energetically more preferred than the equatorial phosphine dissociation by +1.0 kcal/mol for the phosphine cis to the Ru−O bond and by +10.0 kcal/mol for the phosphine cis to the Ru−C_{aryl} bond. Again, the energetically preferred dissociation of the axial phosphine in **2** is due to distortion of the axial phosphine ligand from the axial coordination plane (Figure 3). Unlike **4a**, the η^3-type interaction of the aryl ring into the metal is not observed in **8a** and the orientation of the $-OC_6H_3Me$ moiety in **8a** is very similar to that in **2** (Figure 3). The coordination of the oxygen of CO_2 to **8a** leading to **9a** is a barrierless process (Scheme 5), which can be attributed to the fully developed vacant coordination site in ruthenium, whereas the same process in **4a** required $\Delta G^{\ddagger}$ = +16.6 kcal/mol, mainly to break the η^3 coordination of the aryl ring to the metal. From **9a**, CO_2 inserts into the Ru−C_{aryl} bond via TS_{9a-10a} with $\Delta G^{\ddagger}$ of +23.0 kcal/mol, which is +5.6 kcal/mol higher than the CO_2 insertion into the Ru−O bond via $TS_{9a-10a'}$. It is worth noting that the high-lying Ru−C_{aryl} bond insertion pathway leads to a more stable intermediate **10a** than the low-lying Ru−O bond insertion pathway, giving **10a′**. **10a** is +13.3 kcal/mol more stable than **10a′**. The higher stability of **10a** can be attributed to the η^3 coordination of the $-OC_6H_3Me$ group to the metal, whereas such an interaction is absent in the case of **10a′** (Figure 3). Further, the strain effect is more in **10a′** because of the presence of two four-membered rings. The $\Delta G^{\ddagger}$ value of the forward pathway **9a** → $TS_{9a-10a'}$ → **10a′** and that of its reverse pathway are nearly the same, viz., +1.7 and +2.0 kcal/mol, respectively. This clearly suggests that the low-lying pathway (**9a** → $TS_{9a-10a'}$ → **10a′**) is reversible, and this is only a kinetic phenomenon not favored by the thermodynamic stability of **10a′**. On the other hand, the high-lying pathway leading to **10a** is not easily reversible because of the high $\Delta G^{\ddagger}$ = +20.9 kcal/mol. Further, the phosphine association to **10a** yields the thermodynamically stable product **11a** (−4.5 kcal/mol), wherein CO_2 is inserted into the Ru−C_{aryl} bond. In contrast, the phosphine association to **10a′** does not give the desired product, and instead it releases CO_2 with the formation of the initial complex **2**, which again confirms the reversible reaction from **10a′**. Hence, it is clear that the kinetically favored insertion of CO_2 to the Ru−O bond is not suitable to explain the formation of the product complex, whereas the CO_2 insertion pathway to the Ru−C_{aryl} bond, leading to a thermodynamically stable intermediate **10a**, gives the product complex. This is in agreement with the experimental findings that **11a** is formed in the reaction while the experiments for the CO_2 insertion of the Ru−O bond failed.[25]

We have also tested the possibility of nucleophilic interaction of the oxygen lone pair (from the ligand OC_6H_3Me) of complex **2** and CO_2. If this leads to the formation of a stable O-bound species (Ru−O···CO_2), the subsequent rearrangement will lead to a CO_2 insertion product. Unfortunately, the energy minimization does not yield the O-bound species and, hence, the mechanism via the nucleophilic interaction of oxygen in **2** with the carbon of CO_2 can be discarded.

iii. CO_2 Insertion Reactions of 3. Similar to **1** and **2**, the CO_2 insertion mechanism via the initial phosphine dissociation is

DOI: 10.1021/ic5022577
Inorg. Chem. 2015, 54, 502−512

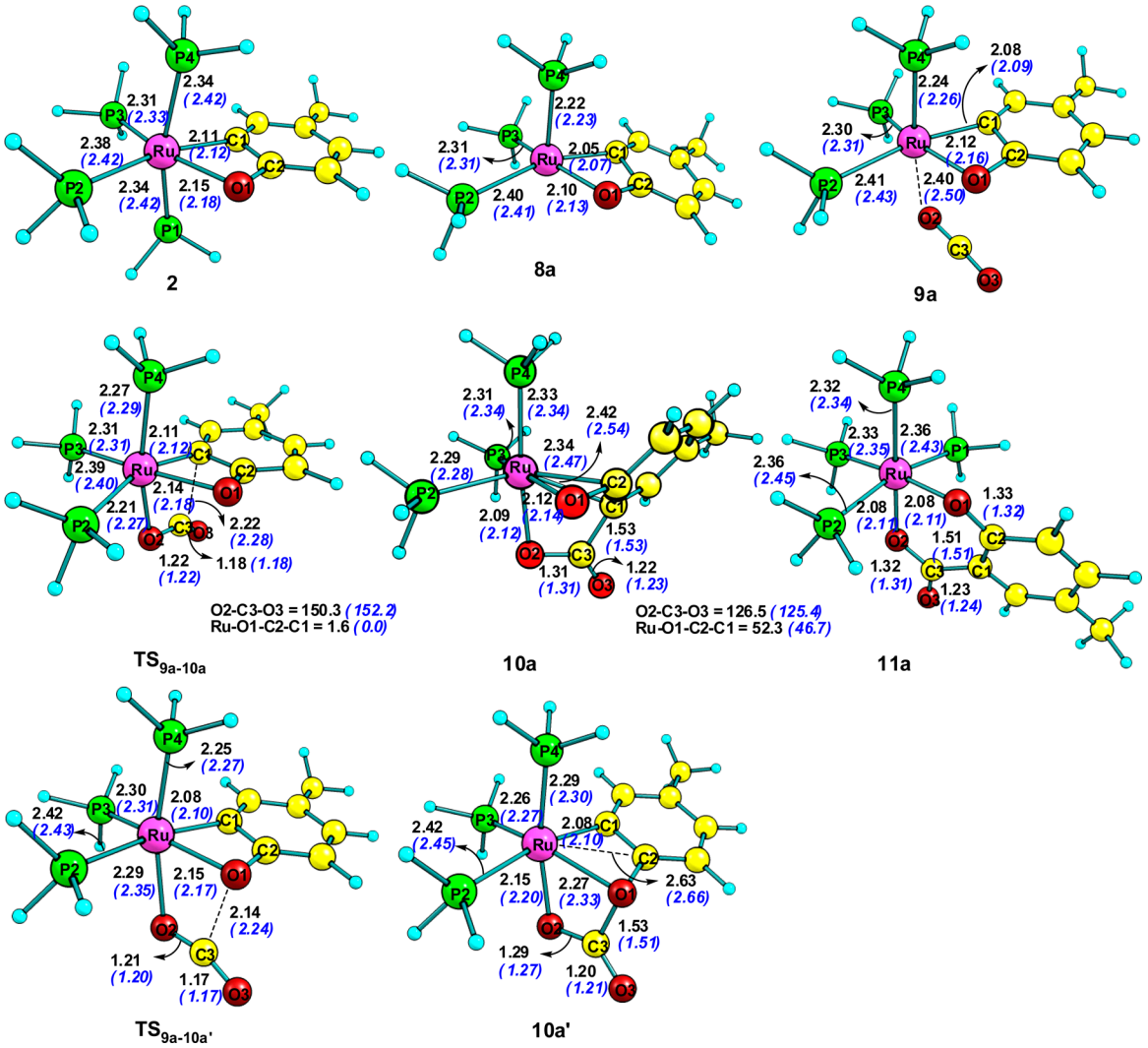

Figure 3. Optimized intermediates and transition states for CO_2 insertion into the Ru−C_{aryl} and Ru−O bonds of **2**, where L = PH_3/PMe_3. Selected distances are given in angstroms.

examined for **3**. The axial phosphine dissociation of **3** gives **14a**, and the ΔG and ΔE values for this step are +6.5 and +18.3 kcal/mol, respectively (Scheme 6). Like in the case of **1** and **2**, the next step is expected to be the coordination of the oxygen of CO_2 to the vacant site of **14a**. However, this does not happen, and instead the Ru···OCO and ligand (N)···CO_2 interactions simultaneously occur without an activation barrier, giving the exothermic Ru−N insertion product **15a** (Figure 4). This is probably due to the nucleophilic affinity of nitrogen toward the carbon of CO_2. The last step of the reaction is the association of phosphine with **15a** to form the desired product **13a**. Unfortunately, this step does not give **13a** and instead leads to the N-bound species **12a** with $\Delta G^{\ddagger}$ of +25.0 kcal/mol. **12a** then undergoes rearrangement to form the desired Ru−N insertion product **13a** with $\Delta G^{\ddagger}$ +19.0 kcal/mol (Figure 4). The CO_2 insertion into the Ru−C_{aryl} bond of **3** via the initial equatorial phosphine dissociation (cis to the Ru−C_{aryl} bond) is also modeled and found to be kinetically less preferred by +17.7 kcal/mol than the CO_2 insertion into the Ru−N via axial phosphine dissociation.

As proposed by the experiments,[29] the rate of CO_2 insertion of **3** is independent of the added phosphine concentration and, hence, the CO_2 insertion of **3** is modeled without prior

Scheme 6. Computed Free Energy Profile (kcal/mol) for CO_2 Insertion into the Ru−N Bond of 3[a]

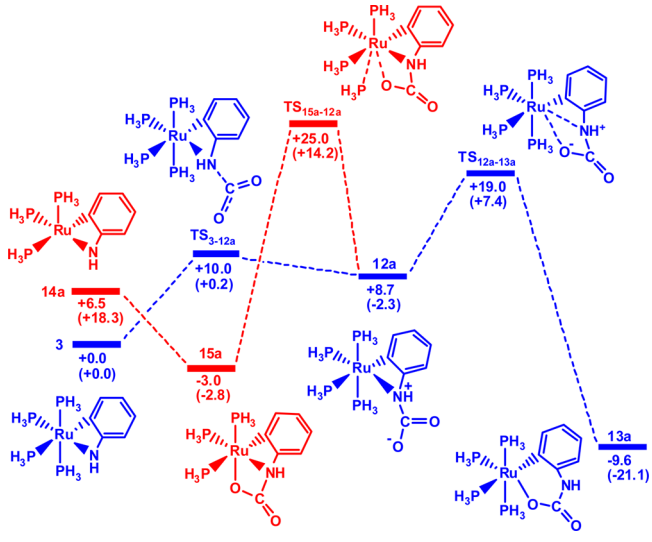

[a]Electronic energies (kcal/mol) are given in parentheses.

DOI: 10.1021/ic5022577
Inorg. Chem. 2015, 54, 502−512

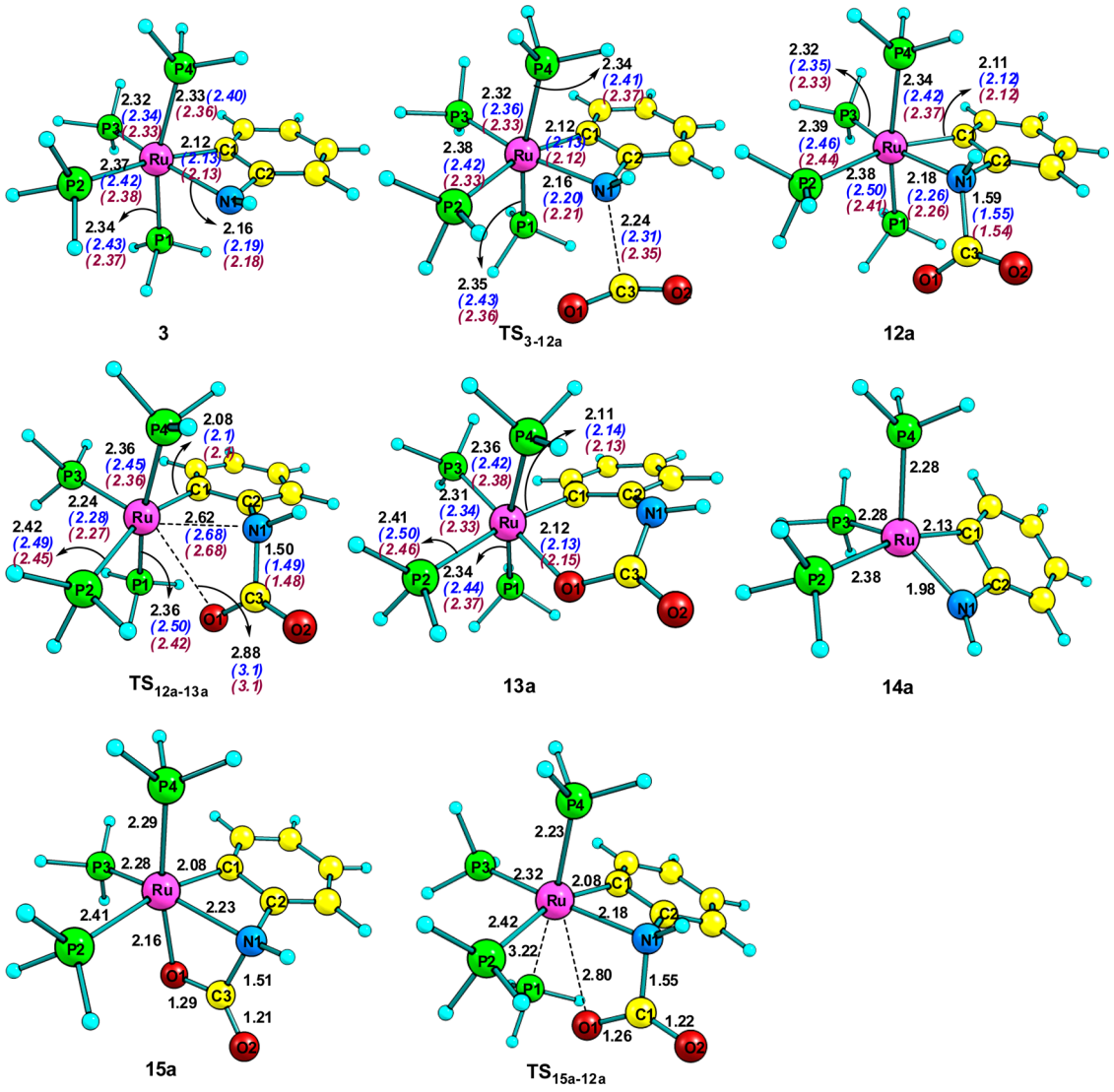

Figure 4. Optimized intermediates and transition states for CO_2 insertion into the Ru−N bond of **3**, where L = PH_3/PMe_3/DMPE. Selected distances are given in angstroms.

dissociation of the phosphine ligand (Scheme 6). Because the metal is coordinatively saturated, this kind of mechanistic possibility arises only if the ligand is capable of directing CO_2 to the metal center. The amido group is well-known for its nucleophilic interaction with CO_2,[21−23] and in the case of **3**, the interaction of the nitrogen lone pair of the $-NHC_6H_4$ moiety on the carbon of CO_2 led to the formation of **12a** by passing through TS_{3-12a} ($\Delta G^{\ddagger}$ = +10.0 kcal/mol; Figure 4). TS_{3-12a} is +15.0 kcal/mol more stable than $TS_{15a-12a}$, suggesting that the proposed pathway by the experimentalists is the most probable pathway (shown in blue in Scheme 6) for the formation of the desired product. The rearrangement of **12a** to **13a** follows the same path as that in the case of the axial phosphine dissociation mechanism via $TS_{12a-13a}$. Because $\Delta G^{\ddagger}$ for the rearrangement of **12a** is +9.0 kcal/mol higher than $\Delta G^{\ddagger}$ of the nucleophilic interaction of the $-NHC_6H_4$ moiety on the carbon of CO_2, the rearrangement becomes the rate-determining step.

The CO_2 insertion mechanism of **1**−**3** shows that participation of the metal center is vital in the case of **1** and **2**, which activates the CO_2 molecule by its coordination into the vacant site of the metal, whereas in **3**, the $-NHC_6H_4$ moiety activates the CO_2 molecule because of the nucleophilic affinity of the nitrogen atom. This result immediately suggests that, by tuning the nucleophilic affinity of the $-NHC_6H_4$ moiety, the CO_2 insertion process can be enhanced. We have tested this hypothesis by calculating the energetics of the transition states TS_{3-12a} and $TS_{12a-13a}$ for three substituted derivatives of **3**, viz., **3**(***p*-Me**), **3**(***p*-OMe**), and **3**(***p*-NMe$_2$**), wherein the substituents −Me, −OMe, and $-NMe_2$ are electron-donating in nature and are located para to the nitrogen of the $-NHC_6H_4$ group (Table 1). The electron-donating substituents in **3**(***p*-Me**), **3**(***p*-OMe**), and **3**(***p*-NMe$_2$**) are expected to increase the nucleophilic affinity of the nitrogen atom of the $-NHC_6H_4$ moiety compared to the unsubstituted species **3**. To further confirm the effect of the substituent on the nitrogen atom of the $-NHC_6H_4$ group, the molecular electrostatic potentials (MESPs) of **3**(***p*-Me**), **3**(***p*-OMe**), and **3**(***p*-NMe$_2$**) are calculated.[59] The MESP minimum value obtained at the lone-pair site of the nitrogen atom (V_{min}) is a quantitative measure of the lone-pair strength of nitrogen or the nucleophilic affinity of the nitrogen atom.[60,61] A higher negative V_{min} indicates the higher nucleophilic affinity of the nitrogen atom.[62] The negative character of V_{min} increased in the order **3**(***p*-Me**), **3**(***p*-OMe**), and **3**(***p*-NMe$_2$**) (Figure 5), which results

DOI: 10.1021/ic5022577
Inorg. Chem. 2015, 54, 502−512

Table 1. Activation Free Energies (kcal/mol) of 3 with Various Substituents and Solvents

complex	activation free energy ($\Delta G^{\ddagger}$, kcal/mol)	
	TS_{3-12a}	$TS_{12a-13a}$
3	+10.0	+19.0
3(*p*-**Me**)	+9.6	+18.0
3(*p*-**OMe**)	+9.6	+17.0
3(*p*-NMe_2)	+9.7	+16.6
	Solvent Effect	
3 in toluene	+9.9	+15.9
3 in THF	+9.9	+13.6
3 in acetone	+9.8	+12.8
3 in acetonitrile	+10.0	+12.6

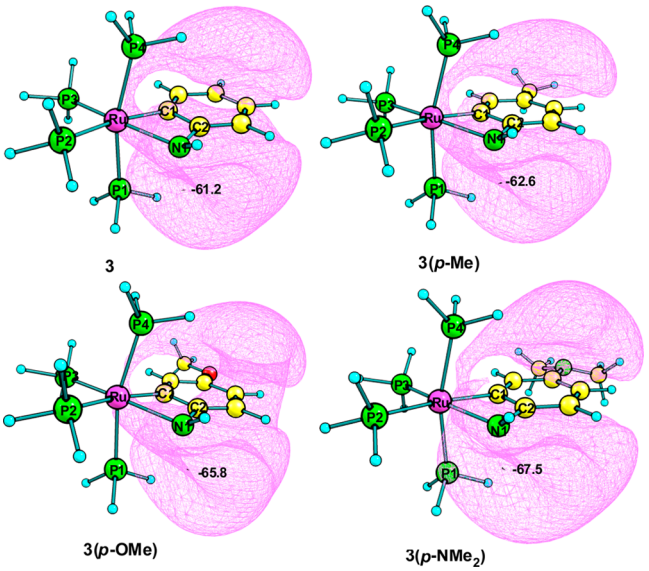

Figure 5. MESP plots of **3**, **3**(*p*-**Me**), **3**(*p*-**OMe**), and **3**(*p*-NMe_2) species. The V_{min} value (kcal/mol) indicates the nitrogen lone-pair strength.

a decrease in the barrier height of transition states in the same order. The electron-donating substitution slightly decreased the $\Delta G^{\ddagger}$ for TS_{3-12a} (decreased by +0.4 kcal/mol), while a more significant decrease in the barrier height was observed for $TS_{12a-13a}$ (decrease by +2.4 kcal/mol).

We have also tested the effect of various solvents such as toluene (ε = 2.4), THF (ε = 7.4), acetone (ε = 20.5), and acetonitrile (ε = 35.7) on the barrier heights (Table 1) of **1**−**3**. Compared to the gas phase, an increase in the polarity of the solvent effectively reduced the activation barrier of the rate-determining step of **3** ($TS_{12a-13a}$) in the order **3** in toluene > **3** in THF > **3** in acetone > **3** in acetonitrile. In the cases of **1** and **2**, the solvent effect is found to be negligible on the energetics. Compared to the $\Delta G^{\ddagger}$ = +19.0 kcal/mol observed for the rate-determining step of the gas-phase reaction of **3**, the best solvent, acetonitrile, gives $\Delta G^{\ddagger}$ = +12.6 kcal/mol for **3** and the best substituent, −NMe_2, gives $\Delta G^{\ddagger}$ = +16.6 kcal/mol for **3**(*p*-NMe_2). These results clearly suggest that a good electron-donating substituent on the aromatic ligand and a polar solvent can significantly reduce the barrier height. In fact, **3**(*p*-NMe_2) in acetonitrile gives the lowest $\Delta G^{\ddagger}$ = +9.9 kcal/mol, which is nearly a 48% reduction in the $\Delta G^{\ddagger}$ value of **3**.

Full Model Systems. The CO_2 insertion reactions of experimentally studied systems $[(PMe_3)_4Ru(\eta^2\text{-}CH_2C_6H_4)]$ [**1**(**PMe**$_3$)], $[(PMe_3)_4Ru(\eta^2\text{-}OC_6H_3Me)]$ [**2**(**PMe**$_3$)], and $[(PMe_3)_4Ru(\eta^2\text{-}NHC_6H_4)]$ [**3**(**PMe**$_3$)] have been computed based on the preferred pathways obtained from simple model systems **1**−**3**. The differences between PMe_3 and its analogues PH_3 complexes are the following. (i) The Ru−P and other coordinated bond distances of **1**(**PMe**$_3$), **2**(**PMe**$_3$), and **3**(**PMe**$_3$) are longer than those of the PH_3 analogues, which can be attributed to the larger steric and trans-influencing character of PMe_3 (Figures 1, 3, and 4) than PH_3.[63,64] (ii) Dissociation of the axial PMe_3 ligand in **1**(**PMe**$_3$) and **2**(**PMe**$_3$) is energetically more favored than dissociation of the axial PH_3 ligand in complexes **1** and **2** by ca. +10.0 kcal/mol (Tables S2 and S3 in the SI). (iii) η^2 coordination of CO_2 exists in **1**(**PMe**$_3$) (Figure S2 in the SI), while it does not exist in the PH_3 analogue. In **1**(**PMe**$_3$), the oxygen of CO_2 coordinates with the ruthenium center, leading to **5a**(**PMe**$_3$), and subsequently it transforms into η^2-coordinated **5a**′(**PMe**$_3$) with an activation barrier +5.1 kcal/mol. From **5a**′(**PMe**$_3$), CO_2 insertion takes place into the Ru−C_{aryl} bond followed by phosphine association to form the final product, whereas in the case of the PH_3 analogue, the insertion was observed directly from **5a**. (iv) The $\Delta G^{\ddagger}$ values for CO_2 insertions of **1**(**PMe**$_3$) and **2**(**PMe**$_3$) through a phosphine dissociative mechanism are found to be lower than those of the corresponding PH_3 complexes, by 10−12 kcal/mol (Table 2). The lowering of the energy barrier is attributed to the energetically favored dissociation of PMe_3 rather than PH_3. In contrast, $\Delta G^{\ddagger}$ for **3**(**PMe**$_3$) via the ligand (NHC_6H_4)-assisted mechanism is slightly higher than the PH_3 analogue by +3.7 kcal/mol. (v) The larger positive entropy contribution of the free PMe_3 ligand than the free PH_3 ligand is responsible for reducing $\Delta G^{\ddagger}$ of **1**(**PMe**$_3$) and **2**(**PMe**$_3$) compared to $\Delta G^{\ddagger}$ of **1** and **2**. This results a larger energy difference between $\Delta E^{\ddagger}(PMe_3)$ and $\Delta G^{\ddagger}(PMe_3)$ in **1**(**PMe**$_3$) (+4.0 kcal/mol) and **2**(**PMe**$_3$) (+3.9 kcal/mol) than those of the PH_3 analogues (+0.8 kcal/mol for **1** and +1.0 kcal/mol for **2**). In **3**, the quantities $\Delta E^{\ddagger}(PMe_3) - \Delta G^{\ddagger}(PMe_3)$ and $\Delta E^{\ddagger}(PH_3) - \Delta G^{\ddagger}(PH_3)$ are almost same for the −NHC_6H_4-assisted mechanism and suggest no favorable entropy contribution from PMe_3. (vi) In all cases, the reaction energies $\Delta E_{RE}(PMe_3)$ and $\Delta G_{RE}(PMe_3)$ are stabilized because of the PMe_3 ligand compared to those of PH_3 analogues.

Table 2. Activation ($\Delta G^{\ddagger}$ and $\Delta E^{\ddagger}$) and Reaction (ΔG_{RE} and ΔE_{RE}) Energies of PH_3- and PMe_3-Based Complexes 1−3[a]

complex	$\Delta G^{\ddagger}(PH_3)$	$\Delta E^{\ddagger}(PH_3)$	$\Delta G^{\ddagger}(PMe_3)$	$\Delta E^{\ddagger}(PMe_3)$	$\Delta G_{RE}(PH_3)$	$\Delta E_{RE}(PH_3)$	$\Delta G_{RE}(PMe_3)$	$\Delta E_{RE}(PMe_3)$
1 (Ru−C_{aryl} bond insertion)	+25.7	+26.5	+13.3	+17.3	−3.2	−14.2	−10.5	−20.6
2 (Ru−C_{aryl} bond insertion)	+23.0	+22.0	+13.4	+17.3	−4.5	−16.3	−13.9	−25.2
3 (Ru−N bond insertion)	+19.0	+7.4	+22.7 (+15.7)	+10.4 (+3.6)	−9.6	−21.1	−11.2 (−10.5)	−23.3 (−21.9)

[a]Energies in kcal/mol. The energetics of the chelating **3**(**DMPE**) complex are shown in parentheses.

DOI: 10.1021/ic5022577
Inorg. Chem. 2015, 54, 502−512

Because the CO_2 insertion mechanism of **3** does not involve phosphine dissociation, the chelating dimethylphosphinoethane (DMPE) ligand is substituted instead of labile phosphines in **3**. Geometric constraints imposed by DMPE have been reported previously to enhance the basicity of a transition-metal center compared to the labile PMe_3 ligand.[65,66] As observed by Holland and Bergman,[66] the modeled DMPE ligand of **3** is tightly bound to the metal center compared to the PMe_3 ligand (Figure 4) and also increased the nucleophilic affinity of the $-NHC_6H_4$ group [V_{min} of **3(DMPE)** = −73.4 kcal/mol, V_{min} of **3(PMe_3)** = −64.0 kcal/mol] compared to that of **3(PMe_3)**. The $\Delta G^{\ddagger}$ value of **3(DMPE)** is found to be +15.7 kcal/mol, which is lower than those of the analogues PH_3 and PMe_3 by +3.3 and +7.0 kcal/mol, respectively. The $-NMe_2$-substituted **3(DMPE)** in acetonitrile further reduced the $\Delta G^{\ddagger}$ value of **3(DMPE)** to +7.3 kcal/mol, which is nearly a 54% reduction in the $\Delta G^{\ddagger}$ value of **3(DMPE)**. This clearly shows that the good choice of an electron-donating substituent, a polar solvent, and a chelating phosphine ligand will enhance the CO_2 insertion of **3**.

CONCLUSIONS

Using the DFT method, we have unraveled the CO_2 insertion into the Ru−C, Ru−O, and Ru−N bonds of **1**−**3** and described the origin of their mechanistic differences. Between the two mechanistic possibilities for **1**, viz., insertion into Ru−C_{aryl} and Ru−CH_2, a clear preference for the former is revealed and ascribed to the enhanced π-type orbital interaction of the aryl ring with the metal center to stabilize the transition state. In **2**, the CO_2 insertion into the Ru−O bond is kinetically more preferred and easier than the insertion into the Ru−C_{aryl} bond. However, the product from the Ru−O bond insertion easily undergoes deinsertion and does not lead to the desired product. Hence, the thermodynamically preferred product from the Ru−C_{aryl} bond is inevitable. In the cases of **1** and **2**, phosphine dissociation is a prerequisite for the CO_2 insertion, whereas in the case of **3**, the insertion reaction proceeds without prior phosphine dissociation. Thus, the first step of CO_2 insertion into the Ru−N bond of **3** is governed by the nucleophilic character of the amido nitrogen. The decrease in the $\Delta G^{\ddagger}$ with an increase in the nucleophilic character of the amido nitrogen via aromatic substitution further confirms the ligand-assisted reactivity of **3** with CO_2. The solvent effects on $\Delta G^{\ddagger}$ are found to be negligible for **1** and **2**, whereas an increase in the polarity of the solvent decreased the $\Delta G^{\ddagger}$ value of **3**. When the electron-donating substituent and polar solvent are combined, $\Delta G^{\ddagger}$ of **3** is reduced by 48%. The chelating-DMPE-incorporated **3(DMPE)** with the electron-donating substituent at the $-NHC_6H_4$ moiety in the polar solvent further reduces the $\Delta G^{\ddagger}$ value of **3** by 62%. This clearly suggest that good choices of chelating phosphine, electron-donating substituent, and polar solvent are vital for modeling the ligand-assisted CO_2 insertion reactions. In the cases of **1** and **2**, the more electron-donating and sterically bulky labile PMe_3 is found to enhance the CO_2 insertion of the Ru−C_{aryl} bond.

ASSOCIATED CONTENT

Supporting Information

Various methods and basis set tests, computed energies and pathways, and optimized intermediates and transition states. This material is available free of charge via the Internet at http://pubs.acs.org.

AUTHOR INFORMATION

Corresponding Author

*E-mail: prabha.vadivelu@niist.res.in or prabha135@gmail.com.

Notes

The authors declare no competing financial interest.

ACKNOWLEDGMENTS

P.V. sincerely thanks the Department of Science & Technology, SERC, for the award of Fast track Young Scientist (Grant CS-232/2012) and also the Director, National Institute for Interdisciplinary Science and Technology (NIIST)-CSIR, Trivandrum, India, for providing the computational facility.

REFERENCES

(1) Arakawa, H.; Aresta, M.; Armor, J. N.; Barteau, M. A.; Beckman, E. J.; Bell, A. T.; Bercaw, J. E.; Creutz, C.; Dinjus, E.; Dixon, D. A.; Domen, K.; DuBois, D. L.; Eckert, J.; Fujita, E.; Gibson, D. H.; Goddard, W. A.; Goodman, D. W.; Keller, J.; Kubas, G. J.; Kung, H. H.; Lyons, J. E.; Manzer, L. E.; Marks, T. J.; Morokuma, K.; Nicholas, K. M.; Periana, R.; Que, L.; Rostrup-Nielson, J.; Sachtler, W. M. H.; Schmidt, L. D.; Sen, A.; Somorjai, G. A.; Stair, P. C.; Stults, B. R.; Tumas, W. *Chem. Rev.* **2001**, *101*, 953.

(2) Gibson, D. H. *Chem. Rev.* **1996**, *96*, 2063.

(3) Leitner, W. *Coord. Chem. Rev.* **1996**, *153*, 257.

(4) Aresta, M.; Quaranta, E.; Tommasi, I. *New J. Chem.* **1994**, *18*, 133.

(5) Jessop, P. G.; Rastar, G.; James, B. R. *Inorg. Chim. Acta* **1996**, *250*, 351.

(6) Yin, X.; Moss, J. R. *Coord. Chem. Rev.* **1999**, *181*, 27.

(7) Urakawa, A.; Jutz, F.; Laurenczy, G.; Baiker, A. *Chem.—Eur. J.* **2007**, *13*, 3886.

(8) Hidai, M.; Hikitaand, T.; Uchida, Y. *Chem. Lett.* **1972**, 521.

(9) Darensbourg, D. J.; Sanchez, K. M.; Reibenspies, J. H.; Rheingold, A. L. *J. Am. Chem. Soc.* **1989**, *111*, 7094.

(10) Simpson, R. D.; Bergman, R. G. *Organometallics* **1992**, *11*, 4306.

(11) Ruiz, J.; Martınez, M. T.; Florenciano, F.; Rodrıguez, V.; Lopez, G. *Inorg. Chem.* **2003**, *42*, 3650.

(12) Yamamoto, T.; Kubota, M.; Yamamoto, A. *Bull. Chem. Soc. Jpn.* **1980**, *53*, 680.

(13) Hartwig, J. F.; Bergman, R. G.; Andersen, R. A. *Organometallics* **1991**, *10*, 3344.

(14) Hartwig, J. F.; Bergman, R. G.; Andersen, R. A. *Organometallics* **1991**, *10*, 3326.

(15) Whittlesey, M. K.; Perutz, R. N.; Moore, M. H. *Organometallics* **1996**, *15*, 5166.

(16) Field, L. D.; Shaw, W. J.; Turner, P. *Chem. Commun.* **2002**, *1*, 46.

(17) Yi, C. S.; Liu, N.; Rheingold, A. L.; Liable-Sands, L. M.; Guzei, I. A. *Organometallics* **1997**, *16*, 3729.

(18) Allen, O. R.; Dalgarno, S. J.; Field, L. D.; Jensen, P.; Willis, A. C. *Organometallics* **2009**, *28*, 2385.

(19) Mandal, S. K.; Ho, D. M.; Orchin, M. *Organometallics* **1993**, *12*, 1714.

(20) Behr, A. *Angew. Chem., Int. Ed.* **1988**, *27*, 661.

(21) Park, S.; Rheingold, A. L.; Roundhill, D. M. *Organometallics* **1991**, *10*, 615.

(22) Schmeier, T. J.; Nova, A.; Hazari, N.; Maseras, F. *Chem.—Eur. J.* **2012**, *18*, 6915.

(23) Dobereiner, G. E.; Wu, J.; Manas, M. G.; Schley, N. D.; Takase, M. K.; Crabtree, R. H.; Hazari, N.; Maseras, F.; Nova, A. *Inorg. Chem.* **2012**, *51*, 9683.

(24) Huang, D.; Makhlynets, O. V.; Tan, L. L.; Lee, S. C.; Rybak-Akimova, E. V.; Holm, R. H. *Proc. Natl. Acad. Sci. U. S. A.* **2011**, *108*, 1222.

(25) Sakaki, S.; Musashi, Y. *Inorg. Chem.* **1995**, *34*, 1914.

(26) Schmeier, T. J.; Nova, A.; Hazari, N.; Maseras, F. *Chem.—Eur. J.* **2012**, *18*, 6915.

DOI: 10.1021/ic5022577
Inorg. Chem. 2015, 54, 502−512

(27) Aresta, M.; Dibenedetto, A.; Pastore, C.; Pápai, I.; Schubert, G. *Top. Catal.* **2006**, *40*, 71.
(28) Field, L. D.; Jurd, P. M.; Magill, A. M.; Bhadbhade, M. M. *Organometallics* **2013**, *32*, 636.
(29) Hartwig, J. F.; Bergman, R. G.; Andersen, R. A. *J. Am. Chem. Soc.* **1991**, *113*, 6499.
(30) Bryndza, H. E. *Organometallics* **1985**, *4*, 1686.
(31) Bryndza, H. E.; Calabrese, J. C.; Reford, S. S. *Organometallics* **1984**, *3*, 1603.
(32) Bryndza, H. E.; Fultz, W. C.; Tam, W. *Organometallics* **1985**, *4*, 939.
(33) Kim, Y. J.; Osakada, K.; Sugita, K.; Yamamoto, T.; Yamamoto, A. *Organometallics* **1988**, *7*, 2182.
(34) Komiya, S.; Akai, Y.; Tanaka, K.; Yamamoto, T.; Yamamoto, A. *Organometallics* **1985**, *4*, 1130.
(35) Becke, A. D. *J. Chem. Phys.* **1992**, *96*, 2155.
(36) Becke, A. D. *J. Chem. Phys.* **1992**, *97*, 9713.
(37) Becke, A. D. *J. Chem. Phys. B* **1993**, *98*, 5648.
(38) Frisch, M. J.; Trucks, G. W.; Schlegel, H. B.; Scuseria, G. E.; Robb, M. A.; Cheeseman, J. R.; Scalmani, G.; Barone, V.; Mennucci, B.; Petersson, G. A.; Nakatsuji, H.; Caricato, M.; Li, X.; Hratchian, H. P.; Izmaylov, A. F.; Bloino, J.; Zheng, G.; Sonnenberg, J. L.; Hada, M.; Ehara, M.; Toyota, K.; Fukuda, R.; Hasegawa, J.; Ishida, M.; Nakajima, T.; Honda, Y.; Kitao, O.; Nakai, H.; Vreven, T.; Montgomery, J. A., Jr.; Peralta, J. E.; Ogliaro, F.; Bearpark, M. J.; Heyd, J.; Brothers, E. N.; Kudin, K. N.; Staroverov, V. N.; Kobayashi, R.; Normand, J.; Raghavachari, K.; Rendell, A. P.; Burant, J. C.; Iyengar, S. S.; Tomasi, J.; Cossi, M.; Rega, N.; Millam, N. J.; Klene, M.; Knox, J. E.; Cross, J. B.; Bakken, V.; Adamo, C.; Jaramillo, J.; Gomperts, R.; Stratmann, R. E.; Yazyev, O.; Austin, A. J.; Cammi, R.; Pomelli, C.; Ochterski, J. W.; Martin, R. L.; Morokuma, K.; Zakrzewski, V. G.; Voth, G. A.; Salvador, P.; Dannenberg, J. J.; Dapprich, S.; Daniels, A. D.; Farkas, Ö.; Foresman, J. B.; Ortiz, J. V.; Cioslowski, J.; Fox, D. J. *Gaussian09*; Gaussian, Inc.: Wallingford, CT, 2009.
(39) Andrae, D.; Häusserman, U.; Dolg, M.; Stoll, H.; Preuss, H. *Theor. Chim. Acta* **1990**, *77*, 123.
(40) Höllwarth, A.; Böhme, M.; Dapprich, S.; Ehlers, A. W.; Gobbi, A.; Jonas, V.; Köhler, K. F.; Stegmann, R.; Veldkamp, A.; Frenking, G. *Chem. Phys. Lett.* **1993**, *208*, 237.
(41) Hehre, W. J.; Ditchfield, R.; Pople, J. A. *J. Chem. Phys.* **1972**, *56*, 2257.
(42) Hariharan, P. C.; Pople, J. A. *Theor. Chim. Acta* **1973**, *28*, 213.
(43) Cancès, M. T.; Mennucci, B.; Tomasi, J. *J. Chem. Phys.* **1997**, *107*, 3032.
(44) Cossi, M.; Barone, B.; Mennucci, B.; Tomasi, J. *J. Chem. Phys. Lett.* **1998**, *286*, 253.
(45) Cossi, M.; Scalmani, G.; Raga, N.; Barone, V. *J. Chem. Phys.* **2002**, *117*, 43.
(46) Perdew, J. P. *Phys. Rev. B* **1986**, *33*, 8822.
(47) Becke, A. D. *Phys. Rev. A* **1988**, *38*, 3098.
(48) Perdew, J. P.; Burke, K.; Ernzerhof, M. *Phys. Rev. Lett.* **1996**, *77*, 3865.
(49) Perdew, J. P.; Burke, K.; Ernzerhof, M. *Phys. Rev. Lett.* **1997**, *78*, 1396.
(50) Adamo, C.; Barone, V. *J. Chem. Phys.* **1999**, *110*, 6158.
(51) Perdew, J. P.; Chevary, J. A.; Vosko, S. H.; Jackson, K. A.; Pederson, M. R.; Singh, D. J.; Fiolhais, C. *Phys. Rev. B* **1993**, *48*, 4978.
(52) Perdew, J. P.; Burke, K.; Wang, Y. *Phys. Rev. B* **1996**, *54*, 16533.
(53) Zhao, Y.; Truhlar, D. G. *J. Phys. Chem. A* **2006**, *110*, 5121.
(54) Zhao, Y.; Truhlar, D. G. *J. Chem. Phys.* **2006**, *125*, 194101.
(55) Grimme, S. *J. Comput. Chem.* **2006**, *27*, 1787.
(56) Ajitha, M. J.; Suresh, C. H. *J. Mol. Catal. A: Chem.* **2011**, *345*, 37.
(57) Pidun, U.; Frenking, G. *Chem.—Eur. J.* **1998**, *4*, 522.
(58) Duarte, F. J. S.; Cabrita, E. J.; Frenking, G.; Santos, A. G. *J. Org. Chem.* **2010**, *75*, 2546.
(59) Kumar, A.; Gadre, S. R.; Mohan, N.; Suresh, C. H. *J. Phys. Chem. A* **2013**, *118*, 526.
(60) Sjoberg, P.; Politzer, P. *J. Phys. Chem.* **1990**, *94*, 3959.
(61) Kumar, A.; Gadre, S. R.; Mohan, N.; Suresh, C. H. *J. Phys. Chem. A* **2013**, *118*, 526.
(62) Mohan, N.; Suresh, C. H.; Kumar, A.; Gadre, S. R. *Phys. Chem. Chem. Phys.* **2013**, *15*, 18401.
(63) Tolman, C. A. *Chem. Rev.* **1977**, *77*, 313.
(64) Sajith, P. K.; Suresh, C. H. *Inorg. Chem.* **2011**, *50*, 8085.
(65) Angelici, R. J. *Acc. Chem. Res.* **1995**, *28*, 5.
(66) Holland, A. W.; Bergman, R. G. *J. Am. Chem. Soc.* **2002**, *124*, 14684.

DOI: 10.1021/ic5022577
Inorg. Chem. 2015, 54, 502−512